ORIGINAL ARTICLE

Leakage beyond the primary lesion: A temporal analysis of cerebrovascular dysregulation at sites of hippocampal secondary neurodegeneration following cortical photothrombotic stroke

Rebecca J. Hood[1,2,3] | Sonia Sanchez-Bezanilla[2,3] | Daniel J. Beard[2,3] | Ruslan Rust[4,5] | Renée J. Turner[1] | Shannon M. Stuckey[1] | Lyndsey E. Collins-Praino[1] | Frederick R. Walker[2,3,6] | Michael Nilsson[3,6,7,8] | Lin Kooi Ong[2,3,9,10]

[1]Discipline of Anatomy and Pathology, School of Biomedicine, Faculty of Health and Medical Sciences, The University of Adelaide, Adelaide, South Australia, Australia

[2]School of Biomedical Sciences and Pharmacy, The University of Newcastle, Callaghan, New South Wales, Australia

[3]Heart and Stroke Research Program, Hunter Medical Research Institute, New Lambton Heights, New South Wales, Australia

[4]Institute for Regenerative Medicine (IREM), University of Zurich, Schlieren, Switzerland

[5]Department of Physiology and Neuroscience, Zilkha Neurogenetic Institute, Keck School of Medicine, University of Southern California, Los Angeles, California, USA

[6]Centre for Rehab Innovations, The University of Newcastle, Callaghan, New South Wales, Australia

[7]School of Medicine and Public Health, The University of Newcastle, Callaghan, New South Wales, Australia

[8]LKC School of Medicine, Nanyang Technological University, Singapore, Singapore

[9]School of Pharmacy, Monash University Malaysia, Bandar Sunway, Selangor, Malaysia

Abstract

We have previously demonstrated that a cortical stroke causes persistent impairment of hippocampal-dependent cognitive tasks concomitant with secondary neurodegenerative processes such as amyloid-β accumulation in the hippocampus, a region remote from the primary infarct. Interestingly, there is emerging evidence suggesting that deposition of amyloid-β around cerebral vessels may lead to cerebrovascular structural changes, neurovascular dysfunction, and disruption of blood–brain barrier integrity. However, there is limited knowledge about the temporal changes of hippocampal cerebrovasculature after cortical stroke. In the current study, we aimed to characterise the spatiotemporal cerebrovascular changes after cortical stroke. This was done using the photothrombotic stroke model targeting the motor and somatosensory cortices of mice. Cerebrovascular morphology as well as the co-localisation of amyloid-β with vasculature and blood–brain barrier integrity were assessed in the cortex and hippocampal regions at 7, 28 and 84 days post-stroke. Our findings showed transient cerebrovascular remodelling in the peri-infarct area up to 28 days post-stroke. Importantly, the cerebrovascular changes were extended beyond the peri-infarct region to the ipsilateral hippocampus and were sustained out to 84 days post-stroke. When investigating vessel diameter, we showed a decrease at 84 days in the peri-infarct and CA1 regions that were exacerbated in vessels with amyloid-β deposition. Lastly, we showed sustained vascular leakage in the peri-infarct and ipsilateral hippocampus, indicative of a compromised blood–brain-barrier. Our findings

[10]School of Health and Medical Sciences & Centre for Health Research, University of Southern Queensland, Toowoomba, Queensland, Australia

Correspondence
Lin Kooi Ong, School of Health and Medical Sciences, University of Southern Queensland, Toowoomba, Queensland, Australia.
Email: lin.ong@usq.edu.au

Cover image for this issue: https://doi.org/10.1111/jnc.15646

indicate that hippocampal vasculature may represent an important therapeutic target to mitigate the progression of post-stroke cognitive impairment.

1 | INTRODUCTION

Over the recent years, our understanding of secondary neurodegeneration (SND) after stroke has expanded based on pre-clinical and clinical findings. Post-stroke SND involves the progressive loss of brain tissue at remote regions connected to the area damaged by the initial infarction that develops within days after the initial stroke and persists for months to years (Baron et al., 2014; Zhang, Zhang, Xing, et al., 2012). Post-stroke SND has been consistently observed in remote regions such as the ipsilateral thalamus, substantia nigra and white matter tracts in both rodent and human studies (Abe et al., 2003; Li et al., 2020; Nakane et al., 1992, 2002). The key features of SND include neuronal loss, neuroinflammation and accumulation of neurotoxic proteins (Ong et al., 2017; Stuckey et al., 2021). This observation is of particular interest as SND shares common pathophysiological features with other neurodegenerative conditions, including tau hyperphosphorylation and amyloid-β deposition (Ong et al., 2017), suggesting a link between SND and the onset of dementia. Indeed, a previous history of stroke is a major risk factor for the development of dementia, with approximately 30% of stroke survivors going on to develop dementia (Barba et al., 2000; Levine et al., 2015).

Our research team has been particularly interested in hippocampal SND after cortical stroke as the hippocampus is known to play a critical role in cognitive function. We recently identified that cortical photothrombotic stroke induces persistent cognitive impairment in various hippocampal-dependent tasks such as associative memory, and cognitive flexibility (Sanchez-Bezanilla et al., 2021; Sanchez-Bezanilla, TeBay, et al., 2019). While the primary infarct was confined to the motor and somatosensory cortices, we demonstrated that the neuropathology changes, including neuronal loss, activation of resident inflammatory cells such as microglia and astrocytes, and increased accumulation of neurotoxic proteins were extended to the ipsilateral hippocampus (Sanchez-Bezanilla et al., 2021; Sanchez-Bezanilla, TeBay, et al., 2019). Interestingly, we showed that the spatial distribution of amyloid-β shifted over time, with a scattered distribution of amyloid-β in the brain parenchyma between 7 and 28 days post-stroke, followed by deposition of amyloid-β around cerebral vessels at 84 days post-stroke (Sanchez-Bezanilla et al., 2021). While previous studies in Alzheimer's disease models have shown that

deposition of amyloid-β around cerebral vessels may lead to cerebrovascular structural changes, neurovascular dysfunction, and disruption of blood–brain barrier (BBB) integrity (Shin et al., 2007; Wang et al., 2021), little is known about the temporal changes of hippocampal cerebrovasculature after cortical photothrombotic stroke.

The neurovascular unit (NVU; including neurons, astrocytes, microglia, pericytes and endothelial cells) plays an important role in regulating and maintaining cerebral homeostasis, cerebral blood flow and inducing the BBB (Iadecola, 2017). Recent research has highlighted the importance of the NVU in acute, subacute and chronic stroke pathophysiology and led stroke researchers to reconsider the important role of the NVU in acute stroke therapy and recovery (Zhang, Zhang, & Chopp, 2012). BBB permeability has been observed in humans to be increased from as early as <6h to more than 30 days post-stroke and is associated with worse clinical outcomes (Bernardo-Castro et al., 2023). Despite the potentially detrimental effect of BBB breakdown on stroke outcomes in the acute phase of stroke, including hemorrhagic transformation and vasogenic oedema (Merali et al., 2017), BBB breakdown is a necessary step for the initiation of angiogenesis within the lesion, which is one of the most important processes for functional recovery after stroke (Zhang & Chopp, 2009). In the subacute phase of stroke (1–3 weeks), angiogenesis begins resulting in newly formed vessels that are leaky in surrounding and remote regions of the initial stroke injury and contribute further to BBB permeability (Rust, 2020). However, BBB permeability in these new vessels gradually decreases after 6 weeks, with the result being larger mature vessels that can restore cerebral blood flow to the previously ischemic areas, paving the way for neurogenesis and functional recovery (Bernardo-Castro et al., 2020).

Several studies have documented the importance of angiogenesis in restoring blood flow within the lesion and promoting functional recovery in both animal models (Hayashi et al., 2003) and in human patients with stroke (Krupinski et al., 1994). However, little is known about temporal changes to angiogenesis, the angioarchitecture and BBB permeability in more distal regions, such as the hippocampus, after cortical stroke and whether these changes are associated with SND processes. This study represents an extension of a previous study carried out by our group (Sanchez-Bezanilla et al., 2021). The aim of the current study was to investigate the

impact of cortical photothrombotic stroke on the cerebrovascular morphological changes within the primary cortical infarction site and ipsilateral hippocampal regions at 7, 28 and 84 days post-stroke. Furthermore, we assessed co-localisation of amyloid-β with vasculature as well as BBB integrity and major tight junction protein and matrix metallopeptidase. The purpose of this hypothesis-generating study was to identify potential mechanisms related to post-stroke SND, which could then be explored in subsequent investigations.

2 | MATERIALS AND METHODS

The data that support the study findings are available from the corresponding author upon reasonable request. See (Sanchez-Bezanilla et al., 2021) for detailed protocols.

2.1 | Experimental design

All animal experiments were approved by the University of Newcastle Animal Care and Ethics Committee (A-2013-340) and conducted in accordance with the New South Wales Animal Research Act and the Australian Code of Practice for the use of animals for scientific purposes. This study represents an extension of a previous study (Sanchez-Bezanilla et al., 2021). Therefore, the materials from the same mouse cohort were used to obtain the data featured in this paper. This is in line with the aim to improve the ethical use of animals in testing according to the 3R principles (Morrissey et al., 2017).

Briefly, C57BL/6 mice (male, 10 weeks old, $n = 85$; RRID:MGI: 2159769) were arbitrarily assigned to cortical photothrombosis ($n = 65$) or sham surgery ($n = 20$). A priori exclusion criteria included no evidence of stroke upon post-mortem examination or death from surgery (see Supplement for excluded animals). Animals were arbitrarily assigned to either PFA or saline perfusion. Brains were collected at 7, 28 and 84 days post-stroke and used for histological (Sham, $n = 10$; 7 days, $n = 9$; 28 days, $n = 9$; 84 days, $n = 12$) or protein analyses (Sham, $n = 10$; 7 days; $n = 8$; 28 days, $n = 8$; 84 days, $n = 11$). Upon brain collection, samples were coded and processed with the researcher blind to animal numbers. All morphological outcome analysis was performed in a blinded manner. For protein analysis, the investigator was blind to specific animal numbers but not group allocation. This study was conducted and reported in accordance with the ARRIVE guidelines (Kilkenny et al., 2010).

It should be noted that the sham group consisted of mice subjected to the sham surgical procedure and euthanased at 84 days post-sham operation. Based on our preliminary data (Jones, 2017), there were no significant changes in the number of neurons and microglia status between sham groups euthanased between 1 and 182 days post-sham operation. Further, previous studies have shown using magnetic resonance neuroimaging that no significant changes occur in the brain volume of sham-operated animals over this period (Feng et al., 2017). Therefore, in this study, we have only included the sham group corresponding to the 84-day time point.

2.2 | Sample size calculation

Sample size was estimated using G*Power 3.1 software. A total of $n = 10$ per group was required, with an estimated standard deviation, SD = 7 and an effect size of Cohen's d = 1.7 allowing a type 1 error of 5% with the power of 80%.

2.3 | Animals

Mice were obtained from the Animal Services Unit at the University of Newcastle. Mice were housed between 2 and 4 per cage in individually ventilated cages throughout the course of the study. Prior to surgery, each cage was arbitrarily assigned to either stroke or sham surgical procedures for the inhabiting mice. Mice were maintained in a temperature (21°C ± 1) and humidity-controlled environment, with a 12:12 h reverse light–dark cycle (lights on 19:00 h). Food and water were available to the mice ad libitum. In all experiments, mice were acclimatised to the environment for a minimum of 7 days prior to the start of the experiment.

2.4 | Photothrombotic occlusion

Photothrombotic occlusion (and sham surgery) was performed as previously described (Pietrogrande et al., 2019; Sanchez-Bezanilla et al., 2021; Sanchez-Bezanilla, Nilsson, et al., 2019; Zhao et al., 2017). Briefly, animals were induced (4%) and maintained (1.5–2.5%) using isoflurane anaesthesia. Immediately following induction, Bupivicaine was administered subcutaneously to the skull (2 mg/kg) to provide long-acting analgesia. To induce stroke, 200 μL of Rose Bengal (10 mg/mL in sterile saline; Sigma Aldrich, USA) or vehicle control was injected intraperitoneally and permitted to circulate for 8 min. In parallel to circulation, an incision was made in the scalp to expose the skull, which was then illuminated by a 4.5 mm diameter cold light source for 15 min, positioned at 2.2 mm lateral to bregma over the left motor and somatosensory cortices. We have taken all the precautions to minimise animal suffering. Animals were continuously monitored throughout surgical procedures by researchers, and depth of anaesthesia was assessed as the absence of the withdrawal reflex of palpebral reflex. The respiratory rate was also continuously monitored. At the conclusion of surgical procedures (before recovery), animals were given a subcutaneous injection of Carprofen (5 mg/kg) and sterile saline (0.9%; 15 mL/kg body weight) to ensure adequate hydration. Animals were monitored daily post-surgery and assessed for any signs of pain, for example, restlessness, vocalisaton, increased respiration, weight loss or facial expressions indicating pain.

2.5 | Tissue processing

Mice were euthanised at 7, 28 or 84 days post-stroke and brains were prepared for histological or protein analyses as previously described

(Sanchez-Bezanilla et al., 2020, 2021; Sanchez-Bezanilla, TeBay, et al., 2019). For histological analysis, mice were deeply anaesthetised using an intraperitoneal injection of sodium pentobarbitol (ca. 200mg/kg) and transcardially perfused with 10mL ice-cold saline (0.9%) followed by 40mL ice-cold paraformaldehyde (4%, pH7.4). Brains were collected and fixed for a further 4h in 4% paraformaldehyde before cryoprotection in 12.5% sucrose in 0.1M PBS. Brains were coronally sectioned at 30μm on a Freezing microtome (Leica, Australia). For Western blotting, mice were deeply anaesthetised using pentobarbitol (I.P.) and transcardially perfused with ice-cold 0.1% diethyloyrocarbonate in 0.9% saline for at least 3min, or until the blood ran clear. Brains were rapidly collected and frozen in −80°C isopentane. Coronal sections were sectioned at 200μm using a cryostat (Leica, Australia) set at −20°C.

2.6 | Immunoflourescence

Free-floating fixed sections (30μm) were labelled for lectin, platelet-derived growth factor receptor β (PDGFRβ), amyloid-β and IgG using previously described methods (Kluge et al., 2017, 2019; Sanchez-Bezanilla et al., 2021). Briefly, sections were rinsed and non-specific binding was blocked using 3% bovine serum albumin. Primary antibodies (PDGFRβ, amyloid-β and IgG) were applied and sections incubated overnight at 4°C, followed by incubation in the corresponding secondary antibodies at 25°C for 2h. Lectin was added in parallel to secondary antibody incubation. See Table 1 for antibodies and concentrations. Brain sections were washed with PBS in between each incubation step. Sections were then mounted and cover slipped.

2.7 | Image quantification

High-resolution images were acquired using a Leica TCS SO8 confocal microscope with Leica HC PLC APO 20×/0.70 and 10×/0.40 objectives for the peri-infarct and hippocampal regions, respectively. Z-stacks (30μm with a step size of 1μm) were taken for each region of interest with imaging parameters maintained throughout imaging sessions (laser power, resolution and gain).

Quantitative analysis was performed on the ipsilateral motor (M1) and somatosensory (S1) cortices (within the peri-infarct territory; Bregma 0.0mm; Figure 1a), as well as the cornu Ammonis 1 (CA1) and dentate gyrus (DG) subregions of the ipsilateral hippocampus (Bregma −1.5; Figure 2a). Vascular images were pre-processed and analysed as previously established with an automated ImageJ (Fiji) script (Rust et al., 2020; Rust, Gronnert, Dogancay, & Schwab, 2019). In brief, images were duplicated, transformed to 8-bit and processed with a median filter to remove noise. Images were then binarised, allocating vascular signal to the value 255 (non-zero pixel) and the background signal value 0 (zero pixel) (see Figure S1). The following parameters were calculated based on the binarised images:

1. *Area fraction (%) of the blood vessels or PDGFRβ+cells*: Area fraction calculation measures the percentage of pixels with non-zero pixels to all pixels.
2. *Vessel length (μm)*: Vessel segment length was assessed by skeletonizing the binary image. This allowed us to tag all pixels in a skeletonised image and then measure their length (μm). The length was normalised per mm^2 of analysed brain tissue.
3. *Number of vascular branches*: The number of branches was assessed by skeletonizing the binary image. This allowed us to identify all its branches. The number of branches was normalised/mm^2 of analysed brain tissue.
4. *Average vessel diameter (μm)*: Fifteen random vessels were sampled from each binary image and manually traced for average vessel diameter. Co-localisation of lectin and amyloid-β labels was used to visualise where both labels overlap for the measurement of amyloid-β positive or negative vessel diameter at 84days post-stroke.

TABLE 1 List of antibodies used for western blot and immunofluorescence analyses.

Target	Sources of antibodies	RRID	Application	Dilution
Amyloid-β	Biolegend, anti-Amyloid-β (6E10), # SIG-39320	AB_662798	IF	1:1000
Claudin 5	Invitrogen, Claudin 5 Polyclonal Antibody, #34-1600	AB_2533157	WB	1:1000
Lectin	Vector Laboratories, DyLight 649 Lycopersicon esculentum (Tomato) lectin (cat no. #DL-1178)		IF	1:1000
MMP9	Abcam, Anti-MMP9 antibody, #ab38898	AB_776512	WB	1:1000
PDGFRβ	Abcam, Recombinant Anti-PDGFR-alpha + PDGFR-beta antibody [Y92] C-terminal, #ab32570	AB_777165	IF	1:1000
β-Actin	Sigma-Aldrich, Monoclonal Anti-β-Actin-HRP antibody, A3854	AB_262011	WB	1:50000
Rabbit IgG	Biorad, anti-rabbit-HRP antibody, #170–6515	AB_11125142	WB	1:7500
	ThermoFisher Scientific, anti-rabbit IgG (H+L) highly cross-adsorbed secondary antibody, Alexa Fluor 488, #A21206	AB_2535792	IF	1:400
Mouse IgG	Biorad, anti-mouse-HRP antibody, #170–6516	AB_11125547	WB	1:10000
	ThermoFisher Scientific, anti-mouse IgG (H+L) highly cross-adsorbed secondary antibody, Alexa Fluor 594, #A21203	AB_141633	IF	1:400

Abbreviations: IF, immunofluorescence; WB, western blot.
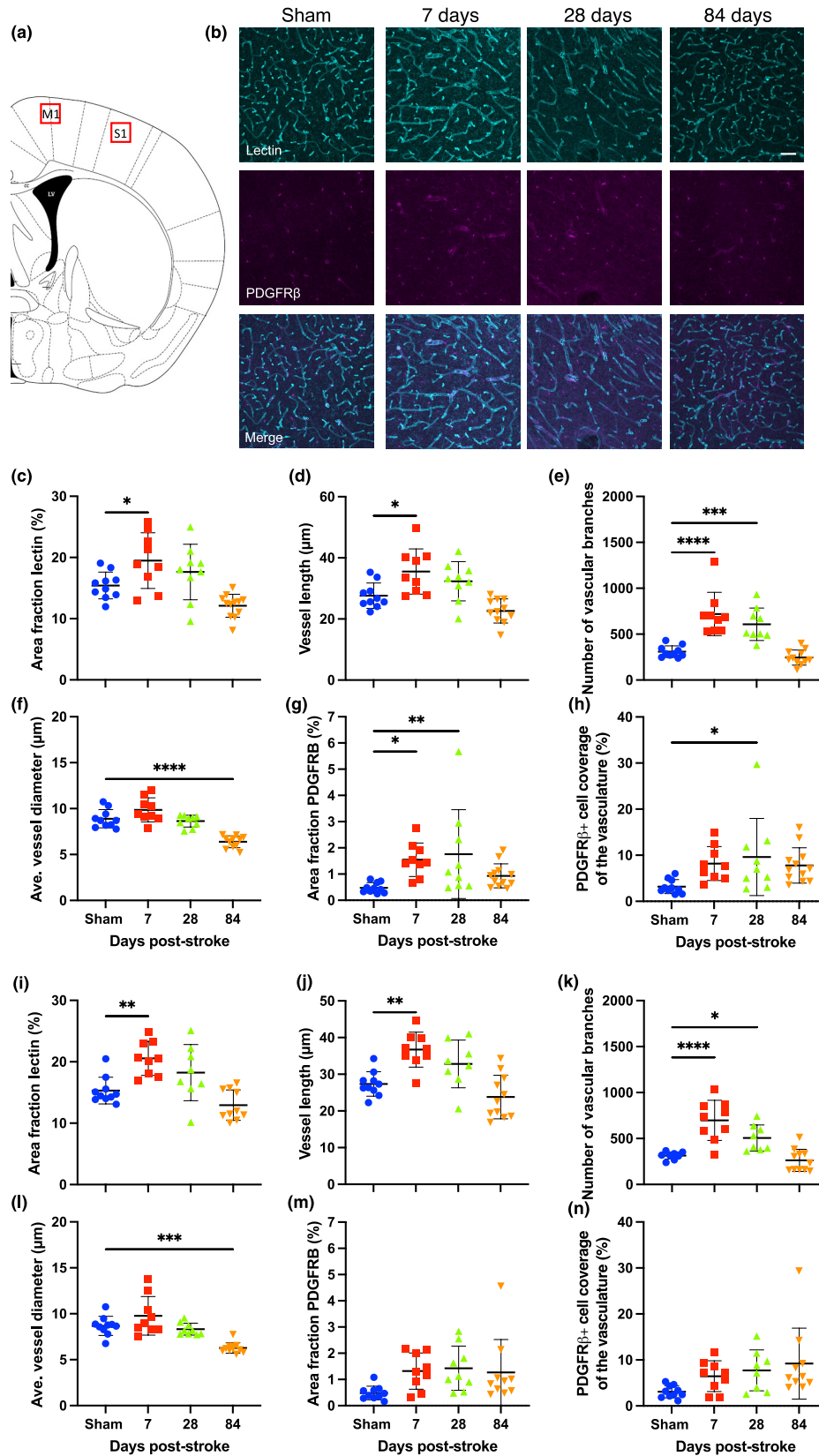
FIGURE 1 Temporal changes in the cerebrovascular morphology of the peri-infarct area after cortical photothrombotic stroke. (a) Schematic shows the location of image analysis in the motor (M1) and sensory (S1) cortices. (b) Representative immunofluorescence labelling for lectin (cyan) and PDGFRβ (magenta) up to 84 days post-stroke. Changes to lectin and PDGFRβ over time in the M1 (c–h; sham, $n = 10$ mice; 7 days, $n = 9$ mice; 28 days, $n = 9$ mice; 84 days, $n = 12$ mice) and S1 regions (i–n; sham, $n = 10$ mice; 7 days, $n = 9$ mice; 28 days, $n = 8$–9 mice; 84 days, $n = 12$ mice). Scale bar = 50 μm. Mean ± SD (One-way ANOVA with Dunnett's multiple comparisons test). $*p < 0.05$. $**p < 0.01$. $***p < 0.001$.
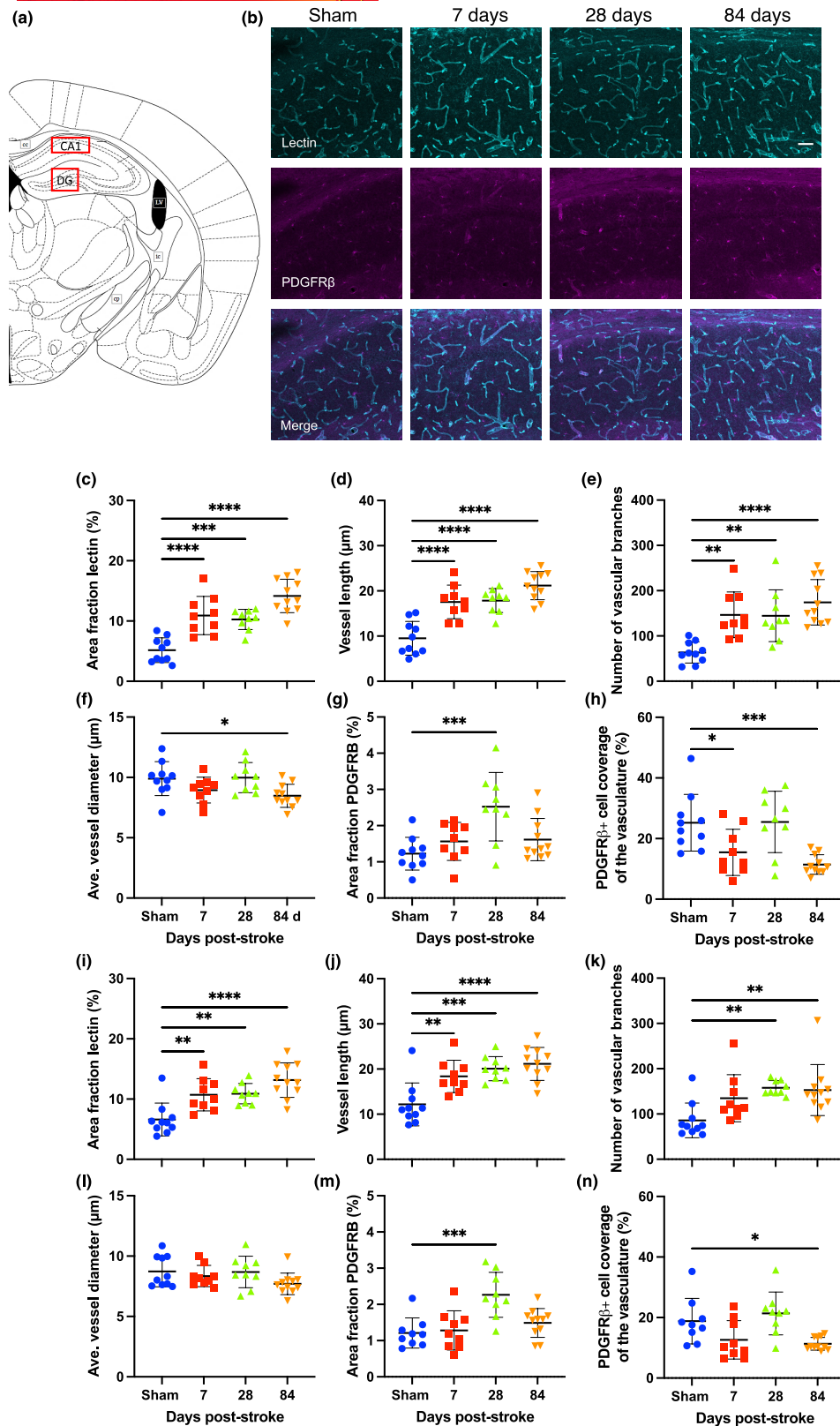
FIGURE 2 Temporal changes in the cerebrovascular morphology of hippocampal subregions after cortical photothrombotic stroke. (a) Schematic shows the location of image analysis in the CA1 and dentate gyrus (DG) of the hippocampus. (b) Representative immunofluorescence labelling for lectin (cyan) and PDGFRβ (magenta) up to 84 days post-stroke. Changes to lectin and PDGFRB over time in the CA1 (c–h; sham, $n = 10$ mice; 7 days, $n = 9$ mice; 28 days, $n = 9$ mice; 84 days, $n = 11$ mice) and DG subregions (i–n; sham, $n = 9$–10 mice; 7 days, $n = 9$ mice; 28 days, $n = 9$ mice; 84 days, $n = 11$ mice). Scale bar = 50 μm. Mean ± SD (One-way ANOVA with Dunnett's multiple comparisons test). *$p < 0.05$. **$p < 0.01$. ***$p < 0.001$.

5. *PDGFRβ+cell coverage of the vasculature (%)*: The PDGFRβ+ cell coverage is quantified by dividing the PDGFRβ area fraction signal from lectin area fraction signal.

For IgG labelling, we performed thresholding analysis as previously described (Johnson & Walker, 2015; Sanchez-Bezanilla et al., 2021; Sanchez-Bezanilla, TeBay, et al., 2019), and investigated the percentage of thresholded material across different pixel intensity thresholds (0–255).

2.8 | Protein extraction and Western blotting

Protein homogenates were obtained from the peri-infarct (Bregma +1.0 to −1.0 mm) and the ipsilateral hippocampus (Bregma −1.2 to −2.5 mm) for Western blot analysis as previously described (Pietrogrande et al., 2019; Sanchez-Bezanilla et al., 2020, 2021; Sanchez-Bezanilla, TeBay, et al., 2019). Briefly, tissue was collected using a 1 mm tissue punch and sonicated in 300 μL lysis buffer (50 mM TRIS buffer pH 7.4, 1 mM EDTA, 1 mM DTT, 80 μM ammonium molybdate, 1 mM sodium pyrophosphate, 1 mM sodium vanadate, 5 mM b-glycerolphosphate, 1 protease inhibitor cocktail tablet, 1 phosphatase inhibitor cocktail tablet, final concentration) and centrifuged at 14 000 G for 20 min at 4°C. The supernatant was collected and protein concentration was quantified using a Pierce BCA protein assay kit (ThermoFisher Scientific, USA) according to manufacturer instructions. Sample buffer (2% SDS, 50 mM Tris, 10% glycerol, 1% DTT, 0.1% bromophenol blue, pH 6.8) was then added to samples. The samples (15 μg of total protein) were then loaded into Biorad Criterion TGX Stain-Free 4–20% gels for electrophoresis. Proteins were transferred from the gels to PVDF membranes, washed in Tris-buffered saline with tween (TBST; 150 mM NaCl, 10 mM Tris, 0.075% Tween-20, pH 7.5) and incubated in 5% skim milk powder in TBST for 1 h at room temperature. Membranes were incubated with primary antibodies (Claudin 5 and matrix metallopeptidase 9 (MMP9)) at 4°C overnight, followed by and secondary antibody for 1 h at room temperature (see Table 1 for antibody concentration). Membranes were washed in TBST between each incubation step. Membranes were visualised on an Amersham Imager 600 using Luminata Classico or Luminata Forte western blotting detection reagents. The density of the bands was measured using Amersham Imager 600 analysis software. See Supplementary Materials for raw western blots.

2.9 | Statistical analysis

Data were analysed using GraphPad Prism v7.02. The primary outcome measure was the difference between the sham and the experimental groups (7, 28 and 84 days post-stroke). Data were tested for normality using the Kolmogorov–Smirnov test and then analysed using a one-way analysis of variance (ANOVA) and corrected for multiple comparisons using Dunnett's post-hoc analysis. Average diameter of amyloid-β positive (Aβ+) vs amyloid-β negative (Aβ-) vessels at 84 days post-stroke was analysed using a two-tailed unpaired

t-test. All data are presented as mean ± SD. Statistical significance was accepted at $p < 0.05$.

3 | RESULTS

3.1 | Cortical photothrombotic stroke causes transient cerebrovascular remodelling in the peri-infarct area

3.1.1 | Lectin

In both peri-infarct regions (M1 and S1), mice exhibited a transient increase in lectin staining, vessel length and number of branches (Figure 1b–e, i–k). Post-hoc testing showed that the area fraction of lectin (%) was significantly higher in both regions at day 7 (M1, $p = 0.0344$; S1, $p = 0.0019$) before returning to sham levels at 28 days. They also exhibited an increase in vessel length (M1, $p = 0.0103$; S1, $p = 0.0013$) and number of branches (M1, $p < 0.0001$; S1, $p < 0.0001$) at 7 days, the latter of which extended out to 28 days post-stroke (M1, $p = 0.0004$; S1, $p = 0.0199$) before returning to sham levels at 84 days. In both regions, average vessel diameter was significantly decreased from sham levels at 84 days post-stroke (M1, $p < 0.0001$; S1, $p = 0.0002$), but not at any of the other time points (Figure 1f, l). See Table 2 for a summary of peri-infarct findings.

3.1.2 | PDGFRβ

There was also a transient increase in PDGFRβ labelling in the M1 region at 7 ($p = 0.0354$) and 28 days ($p = 0.0099$) post-stroke, but no change in the S1 region (Figure 1g, m). The PDGFRβ+ cell coverage of the vasculature was increased in the M1 region at 28 days ($p = 0.0186$) post-stroke, but there were no changes in the S1 region (Figure 1h, n).

3.1.3 | Amyloid-β

At 84 days post-stroke in both regions, mean vessel diameter was significantly reduced in vessels that were co-localised with amyloid-β (M1, 5.1 ± 0.8 μm; S1, 5 ± 0.6 μm) vs those that were not co-localised (M1, 6.8 ± 0.7 μm; S1, 6.5 ± 0.3 μm), $p = 0.0001$ and $p < 0.0001$, respectively (Figure 3a-c).

3.2 | Cortical photothrombotic stroke causes sustained cerebrovascular remodelling in the ipsilateral hippocampus

3.2.1 | Lectin

In the CA1 subregion of the hippocampus, mice exhibited a sustained increase in lectin staining, vessel length and the number of branches

TABLE 2 Summary of findings in the peri-infarct area.

		Motor cortex (M1)		Sensory cortex (S1)	
		Mean ± SD	One-way ANOVA, p value	Mean ± SD	One-way ANOVA, p value
Cerebrovascular remodelling					
Area fraction lectin (%)	Sham	15.4 ± 2.2	$F_{(3,36)} = 9.239, p = 0.0001$	15.3 ± 2.2	$F_{(3,33)} = 11.26, p < 0.0001$
	7 days	19.5 ± 4.6 ↑		20.6 ± 2.8 ↑↑	
	28 days	17.6 ± 4.5		18.2 ± 4.6	
	84 days	12.1 ± 1.9		12.9 ± 2.5	
Vessel length (µm)	Sham	27.6 ± 4.2	$F_{(3,35)} = 10.29, p < 0.0001$	27.4 ± 3.3	$F_{(3,34)} = 11.69, p < 0.0001$
	7 days	35.5 ± 7.4 ↑		36.7 ± 4.8 ↑↑	
	28 days	32.4 ± 6.4		32.8 ± 6.5	
	84 days	22.6 ± 4		23.8 ± 5.9	
No. vascular branches	Sham	309 ± 63	$F_{(3,35)} = 22.42, p < 0.0001$	315 ± 37	$F_{(3,34)} = 18.83, p < 0.0001$
	7 days	720 ± 236 ↑↑↑		697 ± 219 ↑↑↑	
	28 days	608 ± 176 ↑↑↑		506 ± 142 ↑	
	84 days	245 ± 83		262 ± 120	
Ave. vessel diameter (µm)	Sham	8.9 ± 1	$F_{(3,35)} = 26.08, p < 0.0001$	8.7 ± 1	$F_{(3,35)} = 14.81, p < 0.0001$
	7 days	9.9 ± 1.3		9.8 ± 2.1	
	28 days	8.6 ± 0.7 ↓↓↓		8.3 ± 0.7 ↓↓	
	84 days	6.4 ± 0.6		6.3 ± 0.6	
Area fraction PDGFRβ (%)	Sham	0.5 ± 0.2	$F_{(3,36)} = 4.103, p = 0.0103$	0.8 ± 0.3	$F_{(3,34)} = 2.547, p = 0.0722$
	7 days	1.6 ± 0.6 ↑		1.3 ± 0.7	
	28 days	1.8 ± 1.7 ↑↑		1.4 ± 0.8	
	84 days	0.9 ± 4.6		1.3 ± 1.3	
PDGFRβ+ cell coverage of vasculature	Sham	3.2 ± 1.5	$F_{(3,36)} = 3.183, p = 0.0354$	3.1 ± 1.3	$F_{(3,33)} = 2.842, p = 0.0528$
	7 days	8.2 ± 3.7		6.5 ± 3.4	
	28 days	9.6 ± 6.4 ↑		7.7 ± 4.5	
	84 days	7.8 ± 3.8		9.2 ± 7.7	
		Mean ± SD	Two-tailed Unpaired t-test, p value	Mean ± SD	Two-tailed Unpaired t-test, p value
Ave. vessel diameter:lectin+Aβ (µm)	84 days	5.1 ± 0.8	$t_{(18)} = 4.947, p = 0.0001$	5 ± 0.6	$t_{(20)} = 8.351, p < 0.0001$
Ave. vessel diameter:lectin-Aβ (µm)	84 days	6.8 ± 0.7		6.5 ± 0.3	
		Mean ± SD	One-way ANOVA, p value	Mean ± SD	One-way ANOVA, p value
Vascular leakage (IgG) % threshold					
Pixel intensity 210	Sham	0.009 ± 0.007	$F_{(3,35)} = 2.405, p = 0.0839$	0.006 ± 0.006	$F_{(3,35)} = 4.058, p = 0.0142$
	7 days	18 ± 24		20.9 ± 18.8 ↑	
	28 days	4.9 ± 8.4		3.3 ± 4.7	
	84 days	9.4 ± 16.8		16.6 ± 23.5	

TABLE 2 (Continued)

		Mean ± SD	One-way ANOVA, p value	Mean ± SD	One-way ANOVA, p value
Pixel intensity 230	Sham	0.05 ± 0.03	$F_{(3,35)} = 12.7, p < 0.0001$	0.05 ± 0.03	$F_{(3,35)} = 15.15, p < 0.0001$
	7 days	72 ± 18.3 ↑↑↑↑		79.8 ± 20.5 ↑↑↑	
	28 days	45.7 ± 29.1 ↑↑		48.9 ± 16.9 ↑↑↑	
	84 days	37.1 ± 37.2 ↑↑		42.3 ± 42.6 ↑↑	
Pixel intensity 240	Sham	2.4 ± 1.2	$F_{(3,35)} = 56.5, p < 0.0001$	2.2 ± 1.4	$F_{(3,35)} = 52.03, p < 0.0001$
	7 days	98.5 ± 1.2 ↑↑↑↑		99.3 ± 1 ↑↑↑↑	
	28 days	29.1 ± 7.6 ↑↑↑↑		96.9 ± 2.3 ↑↑↑↑	
	84 days	70.8 ± 33.5 ↑↑↑↑		65.4 ± 36.3 ↑↑↑↑	
Pixel intensity 245	Sham	29.3 ± 10.7	$F_{(3,35)} = 152.6, p < 0.0001$	26.9 ± 10	$F_{(3,35)} = 137.6, p < 0.0001$
	7 days	99.9 ± 0.1 ↑↑↑↑		99.9 ± 0.2 ↑↑↑↑	
	28 days	99.6 ± 0.5 ↑↑↑↑		99.9 ± 0.1 ↑↑↑↑	
	84 days	92.6 ± 12.7 ↑↑↑↑		89.7 ± 14.7 ↑↑↑↑	

		Mean ± SD	One-way ANOVA, p value
Peri infarct			
Claudin 5	Sham	1 ± 0.1	$F_{(3,31)} = 26.9, p < 0.0001$
	7 days	1.3 ± 0.6	
	28 days	0.2 ± 0.4 ↓↓↓↓	
	84 days	0.1 ± 0.1 ↓↓↓↓	
MMP9	Sham	1 ± 0.4	$F_{(3,31)} = 65.62, p < 0.0001$
	7 days	9 ± 2.9 ↑↑↑↑	
	28 days	3 ± 0.3 ↑	
	84 days	0.6 ± 0.2	

Note: Arrows show significance and direction = ↑ or ↓ $p < 0.05$; ↑↑ or ↓↓ $p < 0.01$; ↑↑↑ or ↓↓↓ $p < 0.001$; $p < 0.0001$ (one-way ANOVA with Dunnett's post-hoc test).

FIGURE 3 Vessels co-localised with amyloid-β (Aβ+) have significantly reduced vessel diameters at 84 days post-stroke compared to those with no co-localizaiton (Aβ-). (a) Representative immunofluorescence labelling for lectin (cyan), amyloid-β (yellow) and PDGFRβ (magenta). Vessels with amyloid-β deposition (◄, white arrow) show a decrease in vessel diameter compared to vessels without amyloid-β deposition (*, asterisk). Scale bar = 50 μm. Average vessel diameter in vessels ± Aβ in the (b) motor (M1; $n = 10$ mice/group) and (c) sensory (S1; $n = 11$ mice/group) cortices and in the (d) CA1 subregion of the hippocampus ($n = 9$ mice/group). ***$p < 0.001$, ****$p < 0.0001$ assessed via two-tailed unpaired t-test.

(Figure 2b-e). Post-hoc testing showed increases from sham at all time points across the parameters ($p \leq 0.0017$). There was a decrease in average vessel diameter in the CA1 subregion at 84 days post-stroke ($p = 0.0244$), but not at any other time point (Figure 2f). See Table 3 for a summary of the findings in the hippocampus and subregions.

Similarly, in the DG subregion, mice exhibited changes in lectin staining, vessel length and the number of branches (Figure 2i-k). Post-hoc testing showed increases from sham across all time points in both lectin staining ($p \leq 0.0037$) and vessel length ($p \leq 0.0029$). Increases were also observed in the number of branches at 28 days ($p = 0.0032$) and 84 days post-stroke ($p = 0.0041$). There was no change in average vessel diameter (Figure 2l).

3.2.2 | PDGFRβ

Both CA1 and DG subregions also showed a transient increase in PDGFRβ labelling. Post-hoc testing showed elevated levels in both regions at 28 days post-stroke (CA1, $p = 0.0003$ and DG, $p = 0.0002$) (Figure 2g, m). The PDGFRβ+ cell coverage of the vasculature also differed over time in both regions. Post-hoc testing showed a decrease at 7 days ($p = 0.0282$) and 84 days ($p = 0.0009$) post-stroke in the CA1 subregion and at only 84 days in the DG ($p = 0.0235$; Figure 2h, n).

3.2.3 | Amyloid-β

At 84 days post-stroke in the CA1 subregion, mean vessel diameter was significantly reduced in vessels that were colocalised with amyloid-β (6.3 ± 1 μm) versus those that were not co-localised (8.9 ± 1.1 μm), $p = 0.0006$ (Figure 3d).

3.3 | Cortical photothrombotic stroke increases vascular leakage (IgG) in the peri-infarct area and ipsilateral hippocampus

We measured the IgG immunoreactivity using cumulative threshold analysis. The number of pixels occurring at each of the pixel intensities was determined and the pixel intensity values were ranked ordered 0 to 255 along with the corresponding number of pixels that occurred at each value. As expected, a limited immunofluorescence signal was observed within the peri-infarct region and hippocampus in shams. We found a significant increase in IgG immunoreactivity in the M1 region of stroked mice at pixel intensities 230, 240 and 245 at all time points compared to shams ($p < 0.01$). Similar results were obtained for the S1 region, however, a significant increase was also observed 7 days post-stroke at pixel

**TABLE 3** Summary of findings in the hippocampus and sub-regions.

		CA1 subregion Mean±SD	CA1 One-way ANOVA, p value	Dentate gyrus (DG) Mean±SD	DG One-way ANOVA, p value
Cerebrovascular remodelling					
Area fraction lectin (%)	Sham	5.2±2.1	$F_{(3,35)}=23.01, p<0.0001$	6.6±2.7	$F_{(3,35)}=11.70, p<0.0001$
	7 days	10.9±3.2 ↑↑↑		10.7±2.7 ↑↑	
	28 days	10.3±1.7 ↑↑↑		10.9±1.7 ↑↑	
	84 days	14.2±2.8 ↑↑↑↑		13.2±2.9 ↑↑↑	
Vessel length (μm)	Sham	9.5±3.7	$F_{(3,35)}=22.6, p<0.0001$	12.2±4.8	$F_{(3,35)}=11.47, p<0.0001$
	7 days	17.6±3.7 ↑↑↑↑		18.4±3.6 ↑↑	
	28 days	17.9±2.7 ↑↑↑↑		20.1±2.7 ↑↑↑	
	84 days	21.2±3.1 ↑↑↑↑		21.1±3.7 ↑↑↑↑	
No. vascular branches	Sham	64±23	$F_{(3,35)}=10.63, p<0.0001$	86±38	$F_{(3,35)}=5.463, p<0.0035$
	7 days	147±51 ↑↑		135±52	
	28 days	145±57 ↑↑		158±16 ↑↑	
	84 days	174±50 ↑↑↑↑		153±56 ↑↑	
Ave. vessel diameter (μm)	Sham	9.9±1.4	$F_{(3,35)}=3.934, p=0.0161$	8.7±1.3	$F_{(3,35)}=1.945, p=0.1404$
	7 days	9±1.1		8.4±0.9	
	28 days	10±1.3		8.7±1.3	
	84 days	8.5±1 ↓		7.7±0.9	
Area fraction PDGFRβ (%)	Sham	1.2±0.5	$F_{(3,35)}=6.857, p=0.0009$	1.2±0.4	$F_{(3,34)}=8.586, p=0.0002$
	7 days	1.6±0.5		1.3±0.5	
	28 days	2.5±1 ↑↑↑		2.3±0.6 ↑↑↑	
	84 days	1.6±0.6		1.5±0.4	
PDGFRβ+ cell coverage of vasculature	Sham	25.2±9.3	$F_{(3,35)}=8.117, p=0.0003$	18.8±7.5	$F_{(3,34)}=6.245, p=0.0017$
	7 days	15.5±7.6 ↓		12.6±6.3	
	28 days	25.5±10.1		21.4±7.1	
	84 days	11.4±3.2 ↓↓↓		11.3±2.1 ↓	
		Mean±SD	**Two tailed unpaired t-test, p value**	**Mean±SD**	**Two tailed unpaired t-test, p value**
Ave. vessel diameter: lectin+Aβ (μm)	84 days	6.3±1	$t_{(16)}=4.225, p=0.0006$	—	—
Ave. vessel diameter: lectin-Aβ (μm)	84 days	8.9±1.1		—	—

(Continues)

TABLE 3 (Continued)

		Mean ± SD	One-way ANOVA, p value	Mean ± SD	One-way ANOVA, p value
Vascular leakage (IgG) % threshold					
Pixel intensity 210	Sham	0.002±0.003	$F_{(3,35)}=0.4842, p=0.6954$	0.07±0.08	$F_{(3,35)}=1.603, p=0.2062$
	7 days	0.3±0.5		0.04±0.04	
	28 days	0.2±0.4		0.04±0.04	
	84 days	0.4±1.2		0.1±0.2	
Pixel intensity 230	Sham	0.009±0.008	$F_{(3,35)}=1.382, p=0.2643$	0.9±0.2	$F_{(3,35)}=1.343, p=0.2763$
	7 days	5±5.2		1±1	
	28 days	6.1±7.9		1.3±1.2	
	84 days	3.3±10.1		1.6±2.5	
Pixel intensity 240	Sham	0.4±0.4	$F_{(3,35)}=25.67, p<0.0001$	4±3.4	$F_{(3,35)}=3.922, p=0.0163$
	7 days	41.2±14.1 ↑↑↑		16.8±8.8 ↑	
	28 days	47.5±9.1 ↑↑↑↑		17.2±9.4 ↑	
	84 days	15.6±20.2 ↑		12.5±13.4	
Pixel intensity 245	Sham	8.6±3.9	$F_{(3,35)}=26.07, p<0.0001$	23.7±10.1	$F_{(3,35)}=9.248, p<0.0001$
	7 days	78.8±10.1 ↑↑↑↑		16.8±8.8	
	28 days	73.5±16.9 ↑↑↑		47.5±9.1 ↑↑	
	84 days	42.6±32.1 ↑↑		33.7±19.9	

		Mean ± SD	One-way ANOVA, p value
Hippocampus			
Claudin 5	Sham	1±0.4	$F_{(3,31)}=5.524, p=0.0037$
	7 days	1.7±0.4 ↑↑	
	28 days	1.2±0.5	
	84 days	1.2±0.2	
MMP9	Sham	1±0.4	$F_{(3,31)}=7.629, p=0.0006$
	7 days	1.4±0.7	
	28 days	1.7±0.7 ↑	
	84 days	0.7±0.2	

Note: Arrows show significance and direction = ↑ or ↓ $p<0.05$, ↑↑ or ↓↓ $p<0.01$, ↑↑↑ or ↓↓↓ $p<0.001$, ↑↑↑↑ or ↓↓↓↓ $p<0.0001$ (one-way ANOVA with Dunnett's post-hoc test).
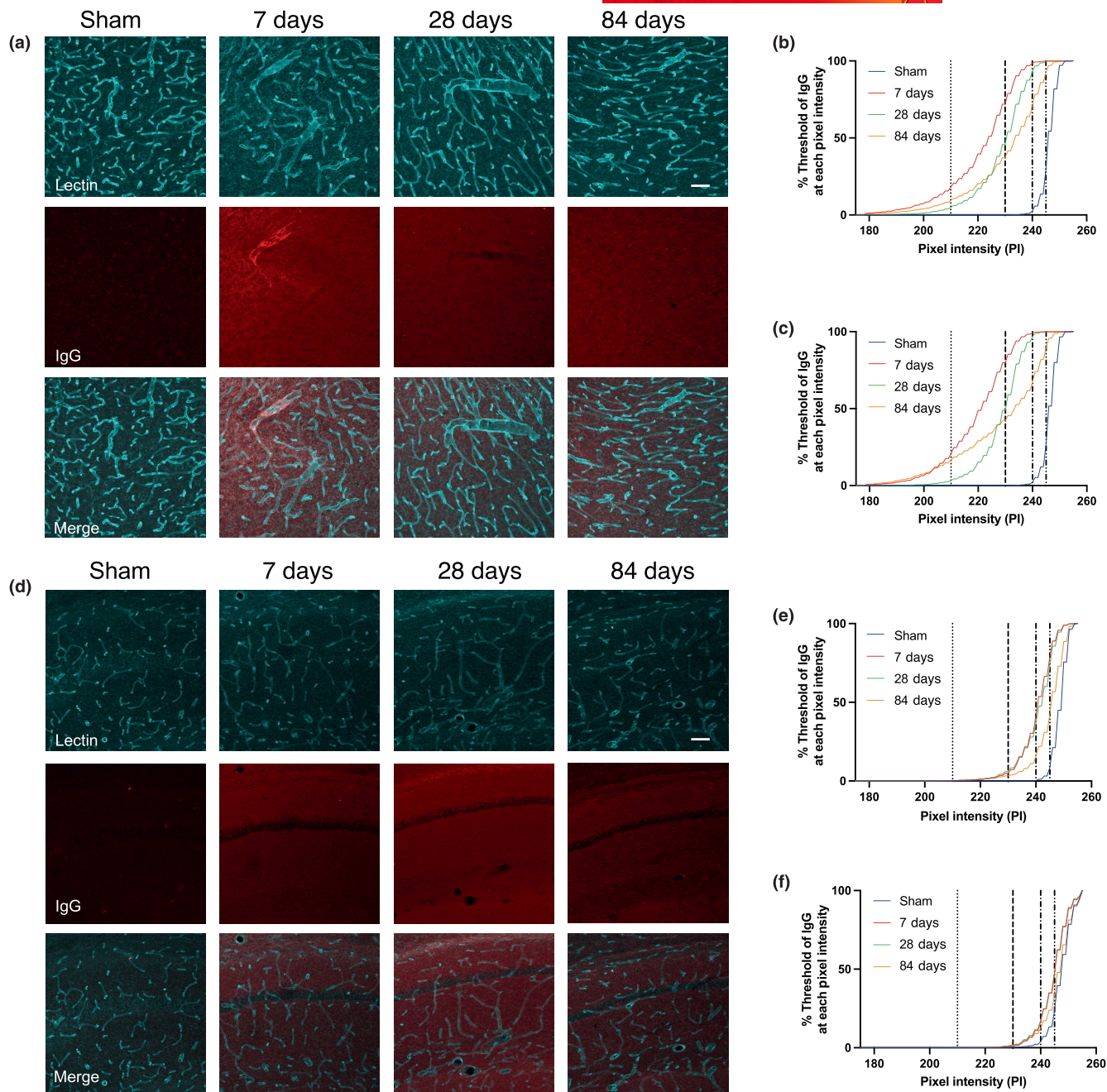
FIGURE 4 Cortical photothrombotic stroke induces BBB leakage in the peri-infarct area (top panel), and ipsilateral hippocampus (bottom panel). Representative immunofluorescence labelling of lectin (cyan) and IgG (red) up to 84 days post-stroke in the peri-infarct area (a) and hippocampus (d) (all regions: sham, $n=10$ mice; 7 days, $n=9$ mice; 28 days, $n=9$ mice; 84 days, $n=11$ mice). Scale bar $=50\,\mu m$. Cumulative threshold analysis shows the mean percentage of IgG in the M1 (b) and S1 (c) cortices; and CA1 (e) and DG (f) subregions of the hippocampus at different levels of pixel intensity (PI). The dotted lines represent the PI levels used in the analysis for detecting genuine differences in immunoreactive signal (refer to Tables 2 and 3 for specific values).

intensity 210 ($p=0.0165$). In the CA1 subregion of the ipsilateral hippocampus, we detected a significant increase in IgG immunoreactivity at pixel intensities 240 and 245 at all time points post-stroke ($p \le 0.0378$). Similarly, in the DG subregion, we observed a transient increase in IgG immunoreactivity at pixel intensities 240 (7 days, $p=0.0176$; 28 days, $p=0.0139$) and 245 (28 days, $p=0.0012$) in stroked mice compared with shams (Figure 4, values presented in Tables 2 and 3).

3.4 | Cortical photothrombotic stroke induces transient changes in the expression of BBB proteins in the peri-infarct area and ipsilateral hippocampus

To assess temporal changes to the BBB, we investigated Claudin 5 (a tight junction protein expressed in endothelial cells; Greene et al., 2019) and MMP9 (an endopeptidase that can degrade the components of extracellular matrix; Greene et al., 2019; Figure 5).
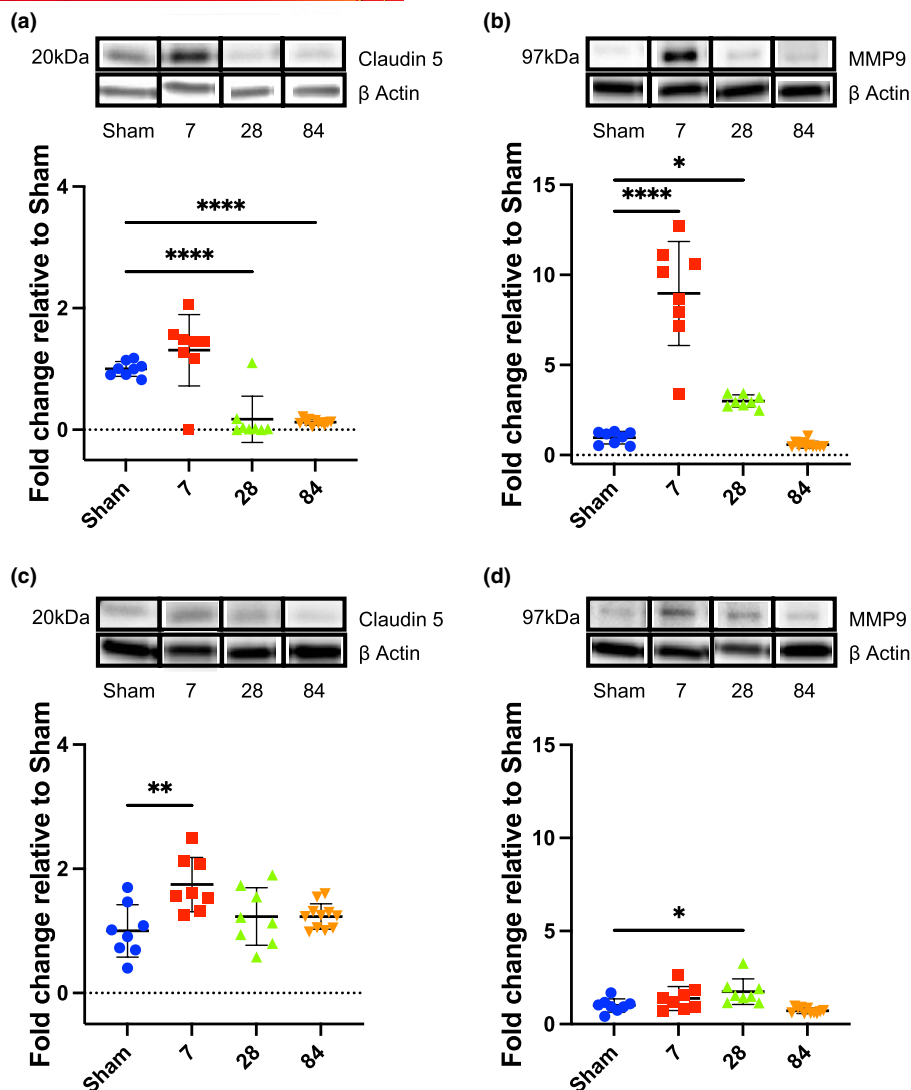
FIGURE 5 Quantification of Claudin 5 and Matrix metalloproteinase 9 (MMP9) in the peri-infarct area ((a) and (b), respectively; top panel) and hippocampus ((c) and (d), respectively; bottom panel) out to 84 days post-cortical photothrombosis (both regions sham, $n = 8$ mice; 7 days, $n = 8$ mice; 28 days, $n = 8$ mice; 84 days, $n = 11$ mice). Representative blots of Claudin 5, MMP9 and β-Actin. Full western blots can be viewed in Figures S2–S5. Loading controls were performed by loading equal amounts of total protein and also were normalised to β-Actin. Levels were expressed as a fold change of mean ± SD for each group relative to the mean of the sham group, shown in the graphs for each protein. $^*p < 0.05$. $^{**}p < 0.01$. $^{***}p < 0.001$. $^{****}p < 0.0001$ assessed via one-way ANOVA with Dunnett's post-hoc test.

In the peri-infarct area, we found the effects of time on the fold change of both proteins. Post-hoc analysis showed significantly decreased levels of Claudin 5 at 28 days and 84 days post-stroke (both $p < 0.0001$). We also observed a transient increase in MMP9, peaking at 7 days post-stroke ($p < 0.0001$) and continuing to be elevated at 28 days ($p = 0.0174$) before returning to sham levels at 84 days. Similarly, in the hippocampus, we found effects of time on both Claudin 5 and MMP9. Claudin 5 transiently increased, peaking at 7 days post-stroke ($p = 0.0013$), before returning to sham levels by 28 days. MMP9 also displayed a transient increase, with fold change peaking at 28 days post-stroke ($p = 0.013$) and returning to sham levels by 84 days.

4 | DISCUSSION

We have previously shown that unilateral cortical photothrombotic stroke causes persistent impairment in associative memory and learning, as well as in cognitive flexibility, up to 84 days post-stroke in this animal cohort (Sanchez-Bezanilla et al., 2021). These deficits were associated with concomitant hippocampal neuropathology, including neuronal loss, microglial activation and the accumulation of amyloid-β. Here we extended upon these findings and characterised the spatiotemporal cerebrovascular changes after cortical stroke. We demonstrated for the first time that cortical photothrombosis causes persistent remote hippocampal cerebrovascular

dysregulation. Specifically, we showed transient cerebrovascular remodelling (vessels and PDGFRβ+ cells) in the peri-infarct areas. Interestingly, the cerebrovascular changes were extended beyond the peri-infarct region to the ipsilateral hippocampus, a site recently documented to undergo SND after cortical stroke, and were sustained out to 84 days post-stroke. When investigating vessel diameter, we showed a decrease at 84 days in the peri-infarct areas and CA1 region that was exacerbated in vessels with amyloid-β deposition. Lastly, we showed sustained vascular leakage in the peri-infarct areas and ipsilateral hippocampus, indicative of a compromised BBB. Collectively, the results of this hypothesis-generating study suggest that cortical stroke induces remote hippocampal cerebrovascular dysregulation, particularly reduction of vessel diameter, as well as BBB leakage, which may partly contribute to the progression of post-stroke SND and cognitive impairment.

In this study, we showed an initial increase in vessel density, vessel length and the number of vascular branches within the peri-infarct areas at 7 days post-stroke. However, these vessel changes had returned to sham levels by 28–84 days post-stroke. Similar increases in peri-infarct blood vessel number have been reported in mice after middle cerebral artery occlusion (MCAo) as early as 2–3 days post-stroke (Hayashi et al., 2003; Marti et al., 2000). Evidence of vascular proliferation out to 4 weeks post-stroke in peri-infarct areas has also been observed in post-mortem tissue samples from stroke patients (Liu, 1988). Further, Krupinski et al. (1994) showed that angiogenesis within the penumbra correlated with longer post-stroke survival in a small number of patients (Krupinski et al., 1994). Although we did not determine whether the vessels were capable of flow, Morris et al. (2022) showed evidence of patency in the peri-infarct region at 2 weeks post-stroke using vascular casting with fluorescein isothiocyanate labelled albumin. Suggesting that at least some of the vessels we observed may be capable of flow. Interestingly, the early changes we observed had resolved by 28–84 days post-stroke. This is consistent with findings by Yu et al. (2007), who showed no differences in the number of microvessels in the peri-infarct area at 30-, 90- and 165-days post-2 h MCAo (Yu et al., 2007). Although we did not study the mechanisms underlying the cerebrovascular changes, previous studies have reported increases in protein and gene expression of angiogenesis-associated markers as early as 1 h post-stroke compared with the contralateral hemisphere, for example, vascular endothelial growth factor (VEGF), flk-1 and angiopoetin-1 (Hayashi et al., 2003; Marti et al., 2000). Interestingly, the up-regulation of many of the markers peaked between 1 and 7 days and then trended downward out to 21 days. The authors did not look beyond this period, so it is unknown whether protein levels returned to contralateral levels. The observed decrease in vessel number in this study may reflect the down-regulation of many of the angiogenesis-associated markers observed in the studies. These newly formed vessels would permit increased blood flow and oxygenation to the affected tissue. We hypothesize that the observed angiogenesis and/or vasculogenesis within the motor cortex may have contributed to the modest improvements in

motor function observed in the animals used in the study (see Sanchez-Bezanilla et al., (2021 for more information). Previous studies have shown similar associations between vascular repair and improvement in motor function after stroke (Rust, Gronnert, Gantner, et al., 2019).

Further, we observed a transient increase in PDGFRβ staining, likely reflecting changes in pericyte number, at 7 and 28 days in the M1 region of the peri-infarct area. This is in line with previous studies. A similar increase in PDGFRβ labelling was observed by Fernandez-Klett et al. (2013) in the lesion site 5-day post-MCAo, remaining elevated out to 28 days (Fernandez-Klett et al., 2013). The authors found an increase in the proliferation of PDGFRβ+ and CD13+ cells peaking at 3 days but remaining elevated out to 28 days post-stroke. A similar pattern of distribution was observed by the authors in 16 post-mortem tissue samples in the acute to chronic stages post-stroke. The significance of these findings is that pericytes, known to express PDGFRβ, are important in new vessel formation as well as functional recovery (Shibahara et al., 2020). Both of which were observed in these animals (Sanchez-Bezanilla et al., 2021).

There is an increasing body of evidence implicating the hippocampus as a site of SND after stroke (Sanchez-Bezanilla et al., 2020, 2021; Sanchez-Bezanilla, TeBay, et al., 2019). In this study, we found persistent increases in vessel density, length and the number of vascular branches out to 84 days post-stroke in the CA1 and DG hippocampal subregions, despite both subregions being remote from the primary infarction. A transient increase in PDGFRβ staining was also observed in the hippocampal subregions, peaking at 28 days post-stroke. Increases in microvascular density have been reported in other areas associated with SND (Zhang, Zhang, Xing, et al., 2012), including the ipsilateral thalamus and substantia nigra (Yanev et al., 2017). Hayward et al. (2011) found evidence of angiogenesis coupled with changes in cerebral blood flow in the ipsilateral thalamus out to 3 months post-stroke (Hayward et al., 2011). However, to our knowledge, this is the first-time changes in cerebrovascular remodelling have been investigated in the ipsilateral hippocampus at a chronic phase post-stroke. Together, these results suggest that post-stroke angiogenesis and/or vasculogenesis may be a common process in remote brain regions implicated in SND, including the hippocampus. Although the specific underlying mechanisms of the remote angiogenesis were beyond the scope of the study, previous studies in the hippocampus have reported early expression changes in the VEGF/VEGFR pathway which precedes neovascularisation after cerebral ischaemia (Marti et al., 2000). Angiogenesis arising from the subventricular zone has been shown to play a role in brain remodelling after 2 h MCAo in rats (Thored et al., 2007). Within the hippocampus the DG contains neural progenitor cells, which are a source of trophic factors, similar to the subventricular zone. Therefore, it is not unreasonable to extrapolate that similar processes are occurring within the hippocampus contributing to the angiogenesis we observed in this study. However, further confirmatory investigation is required.

When investigating vessel diameter, we did not observe any changes out to 28 days post-stroke in any region. In contrast, previous studies found that the vessels present in the peri-infarct area were larger in diameter on average to at least 28 days post-stroke (Morris et al., 2022; Taguchi et al., 2004; Wei et al., 2001). This discrepancy may be explained by previous studies which used a protocol that measured the vessel diameter of perfused fluorescein isothiocyanate labelled gelatin/albumin, whereas, we measured the vessel diameter of lectin-labelled fixed brain sections for this study. We did, however, observe a decrease in average vessel diameter at 84 days in the peri-infarct areas and CA1. To the best of our knowledge, this is the first-ever report of cerebrovascular narrowing in regions at a distance to the primary infarction in the recovery phase of stroke. Amyloid-β oligomers are known to interfere with vascular function (Shin et al., 2007), and we recently reported deposition of amyloid-β around cerebral vessels at 84 days post-stroke in these animals (Sanchez-Bezanilla et al., 2021). Interestingly, we demonstrated that vessels with amyloid-β deposited around their walls were narrower than those without amyloid-β accumulation. Amyloid-β can affect vasomotor regulation by enhancing penetrating arteriole constriction and diminishing vessel dilatation (Dietrich et al., 2010). Further, cerebral capillary narrowing by pericytes has been reported previously following vessel recanalisation in the hyper-acute phase of large vessel stroke (Yemisci et al., 2009) and in response to amyloid-β oligomers in Alzheimer's disease (Nortley et al., 2019). Such reductions in vessel diameter are likely to have profound effects on reducing blood flow, especially in capillary-sized vessels, where the effects of reduced diameter on capillary flow are not accurately estimated by Poiseuille's law and exceed the r^4 effect of vessel radius on flow (Attwell et al., 2010; Johnson, 2023). As we reported previously, persistent neuronal loss was observed in the CA1 out to 84 days post-stroke, along with deficits in hippocampal-dependent tasks (Sanchez-Bezanilla et al., 2021). Based on the present findings, we considered that the delayed reduction of vessel diameter mediated by amyloid-β oligomers in the CA1 subregion of the hippocampus may partly contribute to ongoing cognitive impairment after cortical stroke.

Vascular leakage was increased in the peri-infarct area and ipsilateral hippocampus as measured by IgG extravasation. The IgG labelling suggests that the competence of the BBB in the peri-infarct and hippocampus was compromised. Similar findings out to 1 month post-stroke have been previously reported in the peri-infarct region by us and others using IgG (Zhao et al., 2021) and Evans blue (Weber et al., 2020) extravasation as well as high molecular weight dextran (Yu et al., 2007). BBB disruption has also been observed at different post-stroke timepoints in regions remote from the infarct, including the hippocampus (Weber et al., 2020) and contralateral hemisphere (Garbuzova-Davis et al., 2013). Here, we showed that this leakage persists out to 84 days post-stroke in the peri-infarct area and CA1 subregion of the ipsilateral hippocampus. This may have contributed to the SND and the persistent cognitive deficits observed in this cohort

of animals as reported previously (Sanchez-Bezanilla et al., 2021). While we documented BBB leakage in the peri-infarct area and ipsilateral hippocampus, the mechanisms of BBB dysregulation appeared to be brain region-specific. We hypothesize that the BBB leakage observed in the peri-infarct area is linked with the observed concomitant increase in MMP9 expression early post-stroke and then the decrease in tight junction protein Claudin 5 longer term. However, given that we were using protein homogenates, it is important to confirm this in future studies via protein localisation using immunolabelling. Interestingly as mentioned above, at 84 days post-stroke, we observed the build-up of amyloid-β within the vasculature. Increased levels of amyloid-β oligomers have been shown to influence endothelial permeability and the expression of tight junctions in vitro (Wan et al., 2015). Further investigation is required to determine the specific cause of the protein changes observed here, including tight junction markers, MMPs and tissue inhibitors of metalloproteinases. Unlike the peri-infarct area, there was no difference in either Claudin 5 or MMP9 observed at 84 days in the hippocampus, suggestive of a different underlying mechanism. In the hippocampus, we observed a significant decrease in the PDGFRβ+ cells, likely reflecting a decrease in pericyte coverage of the vasculature at 7 days and 84 days post-stroke in the CA1 subregion and at only 84 days in the DG subregion of the hippocampus compared with sham animals. Pericytes have an important function in the maturity of blood vessels and the integrity of the BBB (Fernandez-Klett et al., 2013; Sun et al., 2021). We hypothesize that the lack of pericyte coverage on the newly formed vessels in the hippocampus may be a contributing factor to the BBB leakage observed in this study. Our hypothesis is supported by Zbesko et al. (2018) who showed similar findings at 7 weeks post-stroke within the infarct core and peri-infarct areas (Zbesko et al., 2018). A key future experiment would be to identify these brain region-specific BBB dysregulation mechanisms to develop targeted therapies for mitigating the progression of hippocampal BBB leakage.

It is important to acknowledge the limitations of this study. Firstly, we used only male mice in this study. Recent evidence from Newton et al. shows that, at least initially, the PT model results in infarcts with similar characteristics across male and female mice (Newton et al., 2022). Another study by Weber et al. characterised BBB disruption out to 3 weeks post-PT stroke and did not observe any sex-related differences in BBB disruption (Weber et al., 2020). Furthermore, we only looked at changes in the ipsilateral regions in the current study; meaning, we may have missed potential stroke-induced changes in the contralateral brain regions. Lastly, although we observed amyloid deposition around the cerebrovasculature at 84 days post-stroke we did not observe the presence of amyloid plaques. We speculate this time point may be too early to see the classic amyloid plaques (Ong et al., 2017). Indeed, previous studies have shown that the amyloid plaques were only observed approximately 9 months post-stroke (Makinen et al., 2008; van Groen et al., 2005). Future studies should be undertaken in both male and female mice as well as in all brain regions to determine

whether these neuropathological changes persist long-term after stroke.

Examples in preclinical studies of treatments that target neurotoxic proteins and cerebrovasculature suggest that therapies aimed at amyloid-β clearance pathway (Ouyang et al., 2021), vascular repair and regeneration (Rust, Gronnert, Weber, et al., 2019) might be quite promising in protecting stroke-induced secondary neurodegeneration, at least in rodent stroke models. Other potential options may be the use of anti-inflammatory drugs that target neuroinflammatory responses of the endothelial cells (Lee et al., 2021; Stuckey et al., 2021). However, while there are several strategies available to target individual aspects of the vasculature and BBB function, studies such as this may help identify targets for a multimodal approach.

In conclusion, we demonstrated that cortical photothrombotic stroke causes cerebrovascular changes that are long term and persistent in the CA1 subregion of the hippocampus, an area critical in cognition. Indeed, we previously demonstrated persistent cognitive impairment and provided critical insights into the underlying mechanisms of SND in the hippocampus in these animals (Figure S6). Interestingly, we showed associations between amyloid-β and reduced vessel diameter, which likely contributed to the persistent neuronal loss and cognitive impairment observed in these animals (Sanchez-Bezanilla et al., 2021). Further exploration into the specific mechanisms underlying post-stroke SND and cognitive impairment is required, however our findings indicate that hippocampal vasculature and BBB function may represent an important therapeutic target to mitigate the progression of post-stroke SND and cognitive impairment.

AUTHOR CONTRIBUTIONS

Rebecca J. Hood: Data curation; formal analysis; investigation; methodology; writing – original draft; writing – review and editing. **Sonia Sanchez-Bezanilla:** Conceptualization; data curation; formal analysis; investigation; methodology; writing – review and editing. **Daniel J. Beard:** Writing – original draft; writing – review and editing. **Ruslan Rust:** Formal analysis; writing – review and editing. **Renée J. Turner:** Writing – review and editing. **Shannon M. Stuckey:** Writing – review and editing. **Lyndsey Collins-Praino:** Writing – review and editing. **Frederick R. Walker:** Conceptualization; funding acquisition; supervision; writing – review and editing. **Michael Nilsson:** Conceptualization; funding acquisition; supervision; writing – review and editing. **Lin Kooi Ong:** Conceptualization; data curation; formal analysis; methodology; supervision; writing – original draft; writing – review and editing.

ACKNOWLEDGEMENTS

CONFLICT OF INTEREST STATEMENT

The author(s) declare no potential conflicts of interest with respect to the research, authorship and/or publication of this article.

PEER REVIEW

The peer review history for this article is available at https://www.webofscience.com/api/gateway/wos/peer-review/10.1111/jnc.16008.

DATA AVAILABILITY STATEMENT

The data that support the study findings are available from the corresponding author upon reasonable request. A preprint of this article was posted on https://www.biorxiv.org/content/10.1101/2023.04.24.538047v1 on April 28, 2023.

ORCID

Rebecca J. Hood https://orcid.org/0000-0001-7485-4883
Sonia Sanchez-Bezanilla https://orcid.org/0000-0003-2753-2691
Daniel J. Beard https://orcid.org/0000-0002-3720-7588
Ruslan Rust https://orcid.org/0000-0003-3376-3453
Renée J. Turner https://orcid.org/0000-0003-4278-8302
Shannon M. Stuckey https://orcid.org/0000-0002-0446-7279
Lyndsey E. Collins-Praino https://orcid.org/0000-0002-4380-7600
Frederick R. Walker https://orcid.org/0000-0002-9068-0761
Michael Nilsson https://orcid.org/0000-0002-8826-1621
Lin Kooi Ong https://orcid.org/0000-0001-8664-0540

TWITTER

Rebecca J. Hood biohazard_hood
Sonia Sanchez-Bezanilla SoniaSanchez92
Daniel J. Beard DocBeardface87
Ruslan Rust rust_ruslan
Renée J. Turner @Neuro_Nay
Shannon M. Stuckey ShannonStuckey
Lyndsey E. Collins-Praino lyndseypraino
Frederick R. Walker @stressmetrics
Lin Kooi Ong DrLinOng

REFERENCES

Abe, O., Nakane, M., Aoki, S., Hayashi, N., Masumoto, T., Kunimatsu, A., Mori, H., Tamura, A., & Ohtomo, K. (2003). MR imaging of postischemic neuronal death in the substantia nigra and thalamus following middle cerebral artery occlusion in rats. *NMR in Biomedicine*, 16(3), 152–159.

Attwell, D., Buchan, A. M., Charpak, S., Lauritzen, M., Macvicar, B. A., & Newman, E. A. (2010). Glial and neuronal control of brain blood flow. *Nature*, 468(7321), 232–243.

Barba, R., Martinez-Espinosa, S., Rodriguez-Garcia, E., Pondal, M., Vivancos, J., & Del Ser, T. (2000). Poststroke dementia: Clinical features and risk factors. *Stroke*, 31(7), 1494–1501.

Baron, J. C., Yamauchi, H., Fujioka, M., & Endres, M. (2014). Selective neuronal loss in ischemic stroke and cerebrovascular disease. *Journal of Cerebral Blood Flow and Metabolism*, 34(1), 2–18.

Bernardo-Castro, S., Sousa, J. A., Bras, A., Cecilia, C., Rodrigues, B., Almendra, L., et al. (2020). Pathophysiology of blood-brain barrier permeability throughout the different stages of ischemic stroke and its implication on hemorrhagic transformation and recovery. *Frontiers in Neurology*, 11, 594672.

Bernardo-Castro, S., Sousa, J. A., Martins, E., Donato, H., Nunes, C., d'Almeida, O. C., et al. (2023). The evolution of blood-brain barrier permeability changes after stroke and its implications on clinical outcome: A systematic review and meta-analysis. *International Journal of Stroke*, 18(7), 783–794. https://doi.org/10.1177/17474930231166306

Dietrich, H. H., Xiang, C., Han, B. H., Zipfel, G. J., & Holtzman, D. M. (2010). Soluble amyloid-beta, effect on cerebral arteriolar regulation and vascular cells. *Molecular Neurodegeneration*, 5, 15.

Feng, Y., Liao, S., Wei, C., Jia, D., Wood, K., Liu, Q., Wang, X., Shi, F. D., & Jin, W. N. (2017). Infiltration and persistence of lymphocytes during late-stage cerebral ischemia in middle cerebral artery occlusion and photothrombotic stroke models. *Journal of Neuroinflammation*, 14(1), 248.

Fernandez-Klett, F., Potas, J. R., Hilpert, D., Blazej, K., Radke, J., Huck, J., et al. (2013). Early loss of pericytes and perivascular stromal cell-induced scar formation after stroke. *Journal of Cerebral Blood Flow and Metabolism*, 33(3), 428–439.

Garbuzova-Davis, S., Rodrigues, M. C., Hernandez-Ontiveros, D. G., Tajiri, N., Frisina-Deyo, A., Boffeli, S. M., et al. (2013). Blood-brain barrier alterations provide evidence of subacute diaschisis in an ischemic stroke rat model. *PLoS One*, 8(5), e63553.

Greene, C., Hanley, N., & Campbell, M. (2019). Claudin-5: Gatekeeper of neurological function. *Fluids and Barriers of the CNS*, 16(1), 3.

Hayashi, T., Noshita, N., Sugawara, T., & Chan, P. H. (2003). Temporal profile of angiogenesis and expression of related genes in the brain after ischemia. *Journal of Cerebral Blood Flow and Metabolism*, 23(2), 166–180.

Hayward, N. M., Yanev, P., Haapasalo, A., Miettinen, R., Hiltunen, M., Grohn, O., et al. (2011). Chronic hyperperfusion and angiogenesis follow subacute hypoperfusion in the thalamus of rats with focal cerebral ischemia. *Journal of Cerebral Blood Flow and Metabolism*, 31(4), 1119–1132.

Iadecola, C. (2017). The neurovascular unit coming of age: A journey through neurovascular coupling in health and disease. *Neuron*, 96(1), 17–42.

Johnson, A. C. (2023). Hippocampal vascular supply and its role in vascular cognitive impairment. *Stroke*, 54(3), 673–685.

Johnson, S. J., & Walker, F. R. (2015). Strategies to improve quantitative assessment of immunohistochemical and immunofluorescent labelling. *Scientific Reports*, 5, 10607.

Jones, K. (2017). *Key mechanisms underlying damage and repair processes in sites of secondary neurodegeneration after ischemic stroke.* University of Newcastle.

Kilkenny, C., Browne, W. J., Cuthill, I. C., Emerson, M., & Altman, D. G. (2010). Improving bioscience research reporting: The ARRIVE guidelines for reporting animal research. *PLoS Biology*, 8(6), e1000412.

Kluge, M. G., Abdolhoseini, M., Zalewska, K., Ong, L. K., Johnson, S. J., Nilsson, M., & Walker, F. R. (2019). Spatiotemporal analysis of impaired microglia process movement at sites of secondary neurodegeneration post-stroke. *Journal of Cerebral Blood Flow and Metabolism*, 39(12), 2456–2470.

Kluge, M. G., Kracht, L., Abdolhoseini, M., Ong, L. K., Johnson, S. J., Nilsson, M., & Walker, F. R. (2017). Impaired microglia process dynamics post-stroke are specific to sites of secondary neurodegeneration. *Glia*, 65(12), 1885–1899.

Krupinski, J., Kaluza, J., Kumar, P., Kumar, S., & Wang, J. M. (1994). Role of angiogenesis in patients with cerebral ischemic stroke. *Stroke*, 25(9), 1794–1798.

Lee, N. T., Ong, L. K., Gyawali, P., Nassir, C., Mustapha, M., Nandurkar, H. H., et al. (2021). Role of purinergic signalling in endothelial dysfunction and thrombo-inflammation in ischaemic stroke and cerebral small vessel disease. *Biomolecules*, 11(7), 994. https://doi.org/10.3390/biom11070994

Levine, D. A., Galecki, A. T., Langa, K. M., Unverzagt, F. W., Kabeto, M. U., Giordani, B., & Wadley, V. G. (2015). Trajectory of cognitive decline after incident stroke. *Journal of the American Medical Association*, 314(1), 41–51.

Li, Z., Gao, H., Zeng, P., Jia, Y., Kong, X., Xu, K., & Bai, R. (2020). Secondary degeneration of white matter after focal sensorimotor cortical ischemic stroke in rats. *Frontiers in Neuroscience*, 14, 611696.

Liu, H. M. (1988). Neovasculature and blood-brain barrier in ischemic brain infarct. *Acta Neuropathologica*, 75(4), 422–426.

Makinen, S., van Groen, T., Clarke, J., Thornell, A., Corbett, D., Hiltunen, M., et al. (2008). Coaccumulation of calcium and beta-amyloid in the thalamus after transient middle cerebral artery occlusion in rats. *Journal of Cerebral Blood Flow and Metabolism*, 28(2), 263–268.

Marti, H. J., Bernaudin, M., Bellail, A., Schoch, H., Euler, M., Petit, E., et al. (2000). Hypoxia-induced vascular endothelial growth factor expression precedes neovascularization after cerebral ischemia. *The American Journal of Pathology*, 156(3), 965–976.

Merali, Z., Huang, K., Mikulis, D., Silver, F., & Kassner, A. (2017). Evolution of blood-brain-barrier permeability after acute ischemic stroke. *PLoS One*, 12(2), e0171558.

Morris, G. P., Gowing, E. K., Courtney, J. M., Coombe, H. E., King, N. E., Rewell, S. S. J., Howells, D. W., Clarkson, A. N., & Sutherland, B. A. (2022). Vascular perfusion differs in two distinct PDGFRbeta-positive zones within the ischemic core of male mice 2 weeks following photothrombotic stroke. *Journal of Neuroscience Research*, 101, 278–292.

Morrissey, B., Blyth, K., Carter, P., Chelala, C., Jones, L., Holen, I., & Speirs, V. (2017). The sharing experimental animal resources, coordinating holdings (SEARCH) framework: Encouraging reduction, replacement, and refinement in animal research. *PLoS Biology*, 15(1), e2000719.

Nakane, M., Tamura, A., Sasaki, Y., & Teraoka, A. (2002). MRI of secondary changes in the thalamus following a cerebral infarct. *Neuroradiology*, 44(11), 915–920.

Nakane, M., Teraoka, A., Asato, R., & Tamura, A. (1992). Degeneration of the ipsilateral substantia nigra following cerebral infarction in the striatum. *Stroke*, 23(3), 328–332.

Newton, J. M., Pushie, M. J., Sylvain, N. J., Hou, H., Weese Maley, S., & Kelly, M. E. (2022). Sex differences in the mouse photothrombotic stroke model investigated with X-ray fluorescence microscopy and Fourier transform infrared spectroscopic imaging. *IBRO Neuroscience Reports*, 13, 127–135.

Nortley, R., Korte, N., Izquierdo, P., Hirunpattarasilp, C., Mishra, A., Jaunmuktane, Z., Kyrargyri, V., Pfeiffer, T., Khennouf, L., Madry, C., Gong, H., Richard-Loendt, A., Huang, W., Saito, T., Saido, T. C., Brandner, S., Sethi, H., & Attwell, D. (2019). Amyloid beta oligomers constrict human capillaries in Alzheimer's disease via signaling to pericytes. *Science*, *365*(6450), eaav9518. https://doi.org/10.1126/science.aav9518

Ong, L., Walker, F., & Nilsson, M. (2017). Is stroke a neurodegenerative condition? A critical review of secondary neurodegeneration and amyloid-beta accumulation after stroke. *AIMS Medical Science*, *4*, 1–16.

Ouyang, F., Jiang, Z., Chen, X., Chen, Y., Wei, J., Xing, S., Zhang, J., Fan, Y., & Zeng, J. (2021). Is cerebral amyloid-beta deposition related to post-stroke cognitive impairment? *Translational Stroke Research*, *12*(6), 946–957.

Pietrogrande, G., Zalewska, K., Zhao, Z., Abdolhoseini, M., Chow, W. Z., Sanchez-Bezanilla, S., Ong, L. K., Johnson, S. J., Nilsson, M., & Walker, F. R. (2019). Low oxygen post conditioning prevents thalamic secondary neuronal loss caused by excitotoxicity after cortical stroke. *Scientific Reports*, *9*(1), 4841.

Rust, R. (2020). Insights into the dual role of angiogenesis following stroke. *Journal of Cerebral Blood Flow and Metabolism*, *40*(6), 1167–1171.

Rust, R., Gronnert, L., Dogancay, B., & Schwab, M. E. (2019). A revised view on growth and remodeling in the retinal vasculature. *Scientific Reports*, *9*(1), 3263.

Rust, R., Gronnert, L., Gantner, C., Enzler, A., Mulders, G., Weber, R. Z., et al. (2019). Nogo-a targeted therapy promotes vascular repair and functional recovery following stroke. *Proceedings of the National Academy of Sciences of the United States of America*, *116*(28), 14270–14279.

Rust, R., Gronnert, L., Weber, R. Z., Mulders, G., & Schwab, M. E. (2019). Refueling the ischemic CNS: Guidance molecules for vascular repair. *Trends in Neurosciences*, *42*(9), 644–656.

Rust, R., Kirabali, T., Gronnert, L., Dogancay, B., Limasale, Y. D. P., Meinhardt, A., et al. (2020). A practical guide to the automated analysis of vascular growth, maturation and injury in the brain. *Frontiers in Neuroscience*, *14*, 244.

Sanchez-Bezanilla, S., Aberg, N. D., Crock, P., Walker, F. R., Nilsson, M., Isgaard, J., et al. (2020). Growth hormone treatment promotes remote hippocampal plasticity after experimental cortical stroke. *International Journal of Molecular Sciences*, *21*(12), 4563. https://doi.org/10.3390/ijms21124563

Sanchez-Bezanilla, S., Hood, R. J., Collins-Praino, L. E., Turner, R. J., Walker, F. R., Nilsson, M., & Ong, L. K. (2021). More than motor impairment: A spatiotemporal analysis of cognitive impairment and associated neuropathological changes following cortical photothrombotic stroke. *Journal of Cerebral Blood Flow and Metabolism*, *41*(9), 2439–2455.

Sanchez-Bezanilla, S., Nilsson, M., Walker, F. R., & Ong, L. K. (2019). Can we use 2,3,5-Triphenyltetrazolium chloride-stained brain slices for other purposes? The application of Western blotting. *Frontiers in Molecular Neuroscience*, *12*, 181.

Sanchez-Bezanilla, S., TeBay, C., Nilsson, M., Walker, F. R., & Ong, L. K. (2019). Visual discrimination impairment after experimental stroke is associated with disturbances in the polarization of the astrocytic aquaporin-4 and increased accumulation of neurotoxic proteins. *Experimental Neurology*, *318*, 232–243.

Shibahara, T., Ago, T., Nakamura, K., Tachibana, M., Yoshikawa, Y., Komori, M., Yamanaka, K., Wakisaka, Y., & Kitazono, T. (2020). Pericyte-mediated tissue repair through PDGFRbeta promotes peri-infarct astrogliosis, Oligodendrogenesis, and functional recovery after acute ischemic stroke. *eNeuro*, *7*(2). https://doi.org/10.1523/ENEURO.0474-19.2020

Shin, H. K., Jones, P. B., Garcia-Alloza, M., Borrelli, L., Greenberg, S. M., Bacskai, B. J., Frosch, M. P., Hyman, B. T., Moskowitz, M. A., & Ayata, C. (2007). Age-dependent cerebrovascular dysfunction in a transgenic mouse model of cerebral amyloid angiopathy. *Brain*, *130*(Pt 9), 2310–2319.

Stuckey, S. M., Ong, L. K., Collins-Praino, L. E., & Turner, R. J. (2021). Neuroinflammation as a key driver of secondary neurodegeneration following stroke? *International Journal of Molecular Sciences*, *22*(23), 13101. https://doi.org/10.3390/ijms222313101

Sun, Z., Gao, C., Gao, D., Sun, R., Li, W., Wang, F., Wang, Y., Cao, H., Zhou, G., Zhang, J., & Shang, J. (2021). Reduction in pericyte coverage leads to blood-brain barrier dysfunction via endothelial transcytosis following chronic cerebral hypoperfusion. *Fluids and Barriers of the CNS*, *18*(1), 21.

Taguchi, Y., Takashima, S., Sasahara, E., Inoue, H., & Ohtani, O. (2004). Morphological changes in capillaries in the ischemic brain in Wistar rats. *Archives of Histology and Cytology*, *67*(3), 253–261.

Thored, P., Wood, J., Arvidsson, A., Cammenga, J., Kokaia, Z., & Lindvall, O. (2007). Long-term neuroblast migration along blood vessels in an area with transient angiogenesis and increased vascularization after stroke. *Stroke*, *38*(11), 3032–3039.

van Groen, T., Puurunen, K., Maki, H. M., Sivenius, J., & Jolkkonen, J. (2005). Transformation of diffuse beta-amyloid precursor protein and beta-amyloid deposits to plaques in the thalamus after transient occlusion of the middle cerebral artery in rats. *Stroke*, *36*(7), 1551–1556.

Wan, W., Cao, L., Liu, L., Zhang, C., Kalionis, B., Tai, X., Li, Y., & Xia, S. (2015). Aβ(1-42) oligomer-induced leakage in an in vitro blood-brain barrier model is associated with up-regulation of RAGE and metalloproteinases, and down-regulation of tight junction scaffold proteins. *Journal of Neurochemistry*, *143*(2), 382–393.

Wang, D., Chen, F., Han, Z., Yin, Z., Ge, X., & Lei, P. (2021). Relationship between amyloid-beta deposition and blood-brain barrier dysfunction in Alzheimer's disease. *Frontiers in Cellular Neuroscience*, *15*, 695479.

Weber, R. Z., Gronnert, L., Mulders, G., Maurer, M. A., Tackenberg, C., Schwab, M. E., et al. (2020). Characterization of the blood brain barrier disruption in the photothrombotic stroke model. *Frontiers in Physiology*, *11*, 586226.

Wei, L., Erinjeri, J. P., Rovainen, C. M., & Woolsey, T. A. (2001). Collateral growth and angiogenesis around cortical stroke. *Stroke*, *32*(9), 2179–2184.

Yanev, P., Seevinck, P. R., Rudrapatna, U. S., Bouts, M. J., van der Toorn, A., Gertz, K., et al. (2017). Magnetic resonance imaging of local and remote vascular remodelling after experimental stroke. *Journal of Cerebral Blood Flow and Metabolism*, *37*(8), 2768–2779.

Yemisci, M., Gursoy-Ozdemir, Y., Vural, A., Can, A., Topalkara, K., & Dalkara, T. (2009). Pericyte contraction induced by oxidative-nitrative stress impairs capillary reflow despite successful opening of an occluded cerebral artery. *Nature Medicine*, *15*(9), 1031–1037.

Yu, S. W., Friedman, B., Cheng, Q., & Lyden, P. D. (2007). Stroke-evoked angiogenesis results in a transient population of microvessels. *Journal of Cerebral Blood Flow and Metabolism*, *27*(4), 755–763.

Zbesko, J. C., Nguyen, T. V., Yang, T., Frye, J. B., Hussain, O., Hayes, M., et al. (2018). Glial scars are permeable to the neurotoxic environment of chronic stroke infarcts. *Neurobiology of Disease*, *112*, 63–78.

Zhang, J., Zhang, Y., Xing, S., Liang, Z., & Zeng, J. (2012). Secondary neurodegeneration in remote regions after focal cerebral infarction: A new target for stroke management? *Stroke*, *43*(6), 1700–1705.

Zhang, L., Zhang, Z. G., & Chopp, M. (2012). The neurovascular unit and combination treatment strategies for stroke. *Trends in Pharmacological Sciences*, *33*(8), 415–422.

Zhang, Z. G., & Chopp, M. (2009). Neurorestorative therapies for stroke: Underlying mechanisms and translation to the clinic. *Lancet Neurology*, *8*(5), 491–500.

Zhao, Z., Hood, R. J., Ong, L. K., Pietrogrande, G., Sanchez Bezanilla, S., Warren, K. E., Ilicic, M., Kluge, M. G., TeBay, C., Ottersen, O. P.,

Johnson, S. J., Nilsson, M., & Walker, F. R. (2021). Exploring how low oxygen post conditioning improves stroke-induced cognitive impairment: A consideration of amyloid-Beta loading and other mechanisms. *Frontiers in Neurology, 12*, 585189.

Zhao, Z., Ong, L. K., Johnson, S., Nilsson, M., & Walker, F. R. (2017). Chronic stress induced disruption of the peri-infarct neurovascular unit following experimentally induced photothrombotic stroke. *Journal of Cerebral Blood Flow and Metabolism, 37*(12), 3709–3724.

SUPPORTING INFORMATION

Additional supporting information can be found online in the Supporting Information section at the end of this article.